VIBRATIONAL ENERGY HARVESTING USING MEMS PIEZOELECTRIC GENERATORS

Andrew Townley – Electrical Engineering, University of Pennsylvania
Advisor: Gianluca Piazza

ABSTRACT

In recent years, energy harvesting using piezoelectric materials has become a very popular research topic. Various device sizes and structures have been tested, but it is difficult to compare power measurements as device fabrication and experimental methods vary from paper to paper. In an effort to standardize comparisons in spite of these changing parameters, the dependence of generator power output on device dimensions has been investigated.

Though MEMS scale devices have been produced, comparatively little work has been done using aluminum nitride (AlN). This project utilizes AlN due to its ease in processing and potential for on-chip integration. By operating at a MEMS scale, the benefit is that arrays of piezo generators can be placed on the same die. With the process advantages of AlN, a long term goal of an integrated power-harvesting chip becomes feasible.

However, theoretical results of scaling predict that raw power output and even power per unit volume will decrease with scaling. This indicates that a single large generator, taking up the same area as several small generators, would produce a noticeably larger power output.

Due to time constraints, no new generators could be fabricated within the time span of the project. An existing piezoelectric cantilever was used to verify the theoretical predictions of resonant frequency and static deflections under applied voltage. These predictions agreed quite closely with the observed results. However, no measurable electrical response could be found while exciting the beam with an electromagnetic shaker device. A similar experiment was performed using an AFM to directly excite the beam, but again the electrical response was difficult to characterize.

While the results of the experiments were not optimal, the difficulty in measuring the electrical response of the beam demonstrates the design challenges involved with energy harvesting on a small scale. Piezoelectric generators rely on resonance to generate useful quantities of power, and power output is highly sensitive to the frequency of the physical vibrations applied. While generators of this type could be useful if targeted to a specific application if the frequency of environmental vibrations is known, a more versatile approach would use a different design to reduce the frequency sensitivity. Broad-band designs, using either non-resonant or self-tuning structures, would be able to harvest energy much more efficiently in changing environments.

1. INTRODUCTION

Low-power wireless distributed sensor networks are becoming attractive for monitoring different variables – such as temperature, strain in a material, or air pressure – over a wide area. However, one drawback of these networks is the power each node draws, though recent work has shown this can be lowered considerably [1]. Batteries can be used to power nodes for extended periods of time, but they have a limited life cycle and eventually need to be replaced. As this can be a costly and time consuming procedure for networks with many nodes, a means of powering the devices indefinitely would be a more practical solution.

Solar power provides a considerable amount of energy per area and volume, but unfortunately is limited to applications that are reliably sunlit [2]. A promising alternative takes advantage of the energy in ambient vibrations and converts it to electrical power. This approach compares very favorably with batteries, providing equal or greater power per unit volume.

There are multiple techniques for converting vibrational energy to electrical energy. The most prevalent three are electrostatic, electromagnetic, and piezoelectric conversion [3]. A majority of current research has been done on piezoelectric conversion due to the low complexity of its analysis and fabrication. Most research, however, has targeted a specific device scale [4-7]. Little research comparing power output across different scales has been done for piezo harvesters, though scaling effects have been discussed briefly in some works [4,8].

This paper aims to develop a theoretical understanding behind the scaling of piezoelectric cantilever generators, and to recommend a direction for future research in this area based on the conclusions.

2. BACKGROUND

2.1 The Piezoelectric Effect

The piezoelectric effect, in essence, is the separation of charge within a material as a result of an applied strain. This charge separation effectively creates an electric field within the material and is known as the direct piezoelectric effect. The converse piezoelectric effect is the same process in reverse: the formation of stresses and strains in a material as a result of an applied electric field.

The IEEE standard on piezoelectricity lists several different forms for the piezoelectric constitutive equations [9]. The form used here is known as the d-form, and the equations are as follows:

$$S = s^E T + dE$$

$$D = dT + \varepsilon^T E$$

These equations, known as the "coupled" equations, reduce to the well-known stress-strain relationship at zero electric field, and the electric field and charge displacement relationship at zero stress.

2.1.1 Piezoelectric Materials

A majority of piezoelectric generators that have been fabricated and tested use some variation of lead zirconate titanate (PZT). Typically, PZT is used for piezoelectric energy harvesters because of its large piezoelectric coefficient and dielectric constant, allowing it to produce more power for a given input acceleration [10]. Another less common material is aluminum nitride (AlN). Though it has a smaller piezoelectric coefficient and dielectric constant, aluminum nitride has advantages in material deposition and in compatibility with the standard CMOS processes used for fabrication of integrated circuits [6]. This makes the possibility of an integrated "power chip" realizable. Because of these advantages, the project will focus on the use of AlN as the piezoelectric material of choice. However, for future optimizations, the change in output power from switching to a different material should be investigated.

2.1.2 Anisotropic Effects and Coupling Modes

Piezoelectric materials have a built-in polarization, and therefore respond differently to stresses depending on the direction. There are two primary modes of electromechanical coupling for piezoelectric materials: the 3-1 mode and the 3-3 mode. In the 3-1 mode (Figure 2.1a), the electric field is produced on an axis orthogonal to the axis of applied strain, but in the 3-3 mode (Figure 2.1b), the electric field produced is on the same axis as the applied strain.

Figure 2.1a:

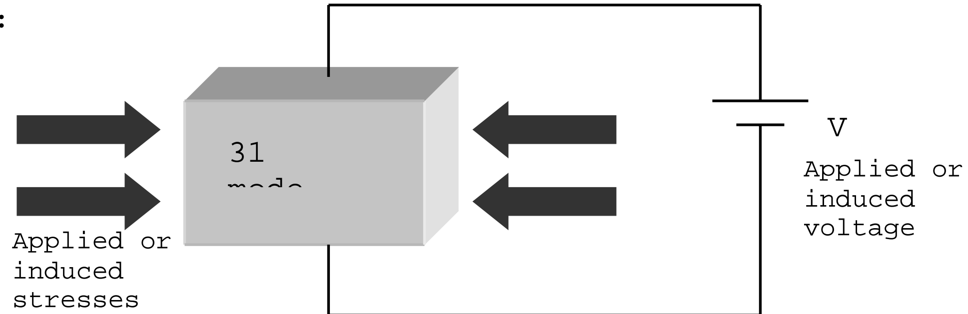

Figure 2.1b:

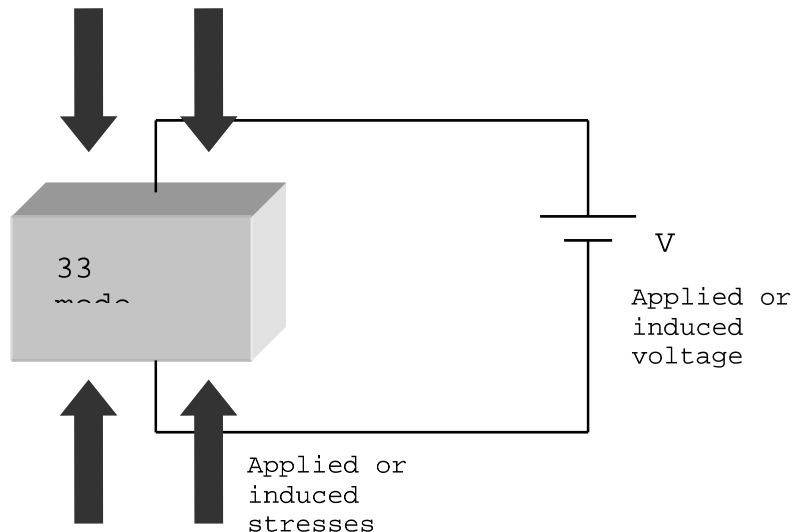

While the piezoelectric coefficient is higher in the 3-3 mode for most materials, taking advantage of the larger coefficient requires a much more complex design. Instead of simple planar electrodes, a series of interdigitated electrodes (IDE) can be used to take advantage of the 3-3 coupling mode [7]. However, this approach leads to a very small device capacitance and therefore a high output impedance, making load matching difficult [11]. Another disadvantage is that the IDE approach only works for electrically-poled piezoelectrics such as PZT. In AlN, the direction of polarization of the material is set during deposition, so fabrication of a 3-3 mode device would be prohibitively complex. For this reason, the devices analyzed in this report will only utilize the 3-1 coupling mode.

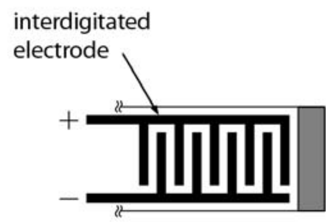

Figure 2.2: an example of an IDE pattern [7]

2.2 Device Configuration

The vast majority of piezoelectric energy harvesting devices use a cantilever beam structure. A cantilever beam, by definition, is a beam with a support only one end, and is often referred to as a “fixed-free” beam. When the generator is subjected to vibrations in the vertical direction, the support structure will move up and down in sync with the external acceleration. The vibration of the beam is induced by its own inertia; since the beam is not perfectly rigid, it tends to deflect when the base support is moving up and down (see Figure 2.3). Typically, a proof mass is added to the free end of the beam to increase that deflection amount. This lowers the resonant frequency of the beam and increases the deflection of the beam as it vibrates. The larger deflection leads to more stress, strain, and consequently a higher output voltage and power [5].

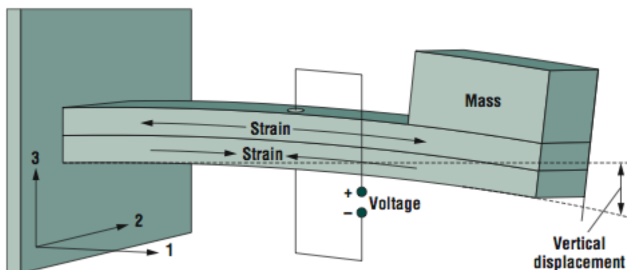

Figure 2.3: note that strain is generated along the length of the beam, hence the use of the 3-1 mode (Figure taken from [13])

Electrodes covering a portion of the cantilever beam are used to conduct the electric charges produced to an electrical circuit, where they can be utilized to charge a capacitor or drive a load. Different electrode lengths or shapes have been shown to affect the output voltage, since strain is not uniform across the beam [12].

2.3 Modes of Vibration and Resonance

A cantilever beam can have many different modes of vibration, each with a different resonant frequency. The first mode of vibration has the lowest resonant frequency, and typically provides the most deflection and therefore electrical energy. A lower resonant frequency is desirable, since it is closer in

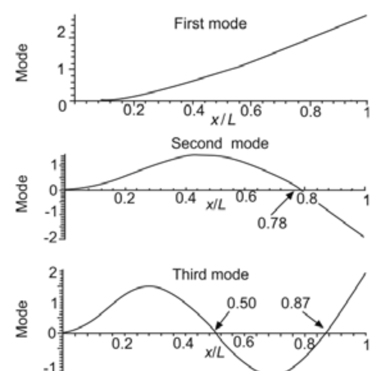

Figure 2.4: Different mode shapes of a vibrating beam. (Figure from [14])

frequency to physical vibration sources and generally more power is produced at lower frequencies [5]. Therefore, energy harvesters are generally designed to operate in the first resonant mode.

Each mode of vibration has a characteristic mode shape. This describes the deflection of the beam along its length. Figure 2.4 shows some examples of mode shapes for the first three vibrational modes of a beam. When a beam is vibrating in a particular mode, the deflection will vary sinusoidally with time, with the amplitude of the sine wave along the length of the beam given by the mode shape. The points where the mode shape is zero are stationary and are referred to as nodes. In general, the *n*th vibrational mode will have *n* nodes.

2.4 Physical Vibration Sources

The frequency and amplitude characteristics of ambient vibration sources have been analyzed in Roundy *et al* [2]. They concluded that most ambient vibration sources have relatively low frequencies (under 200 Hz) and widely varying acceleration levels. As a representative source, they chose the 120 Hz, 2.5 m/s^2 acceleration measured from a microwave oven.

2.5 Rectification and Storage

To convert the AC output voltage to a more useful DC voltage, some form of rectification must be used. One group has come up with a generator that produces DC voltage directly, without the need for rectification, but it is still in the development phase [15]. Typically, low-power or small signal diodes are used to form a bridge rectifier [4-7]. Novel approaches have included the use of custom low-power diodes and voltage multipliers [6].

After rectification, the DC voltage is used to charge a capacitor or battery. This allows the device to draw more power over a short period than the harvester is able to provide. DC-DC conversion schemes have also been explored and have been shown to charge batteries far more efficiently [16].

3. THEORETICAL PREDICTIONS

3.1 Estimation of Resonant Frequency

The following estimates assume that beams are homogenous, composed of a single uniform material, and of constant cross section. However, equivalent values for Young's modulus and density can be calculated for composite beams by using a weighted average method [17]. The resulting equations describing the resonant frequencies are much more compact, making the scaling analysis far more straightforward.

3.1.1 Using the Beam Equation[1]

[1] This information is paraphrased from "The Encyclopedia of Vibration", pages 137-143.

The resonant frequencies of a beam can be estimated using Euler-Bernoulli beam theory [14]. By solving the Euler-Bernoulli beam equation with the appropriate boundary conditions, the eigenvalues of the system can be determined, which then allow for the calculation of the resonant frequencies. The differential equation describing the motion of an Euler-Bernoulli beam is:

$$\frac{\partial^4 \delta}{\partial x^4} + \frac{\rho A}{EI}\frac{\partial^2 \delta}{\partial t^2} = 0,$$

where δ is the beam deflection as a function of position along the beam and time, ρ is the density, A is the area of the cross section of the beam, E is the Young's modulus, and I is the area moment of inertia. For a beam of rectangular cross section, the relevant moment is $I = \frac{1}{12} w t^3$.

The general solution for sinusoidal vibration is as follows, with the constants and eigenvalues determined by the boundary conditions.

$$\delta(x,t) = \left(c_1 \sin\beta x + c_2 \cos\beta x + c_3 \sinh\beta x + c_4 \cosh\beta x\right) \cdot \sin\omega t$$

where

$$\beta^4 = \frac{\rho A \omega^2}{EI}$$

For a fixed-free beam with no proof mass, the relevant boundary conditions for a beam of length L are: $\delta(0,t) = \delta_x(0,t) = 0$ and $\delta_{xx}(L,t) = \delta_{xxx}(L,t) = 0$. These first two boundary conditions indicate that the fixed end of the beam is stationary, and that the beam is flat at the point of attachment. The free end conditions mean that there are no forces applied at that point and no bending moment. The first nontrivial eigenvalue of this system is $\beta L \approx 1.875$, so the equation for the resonant frequency of the first mode is:

$$f = \frac{\omega}{2\pi} = \frac{1.875^2}{2\pi L^2}\sqrt{\frac{EI}{\rho A}}$$

By rewriting I and A in terms of the beam dimensions, the widths cancel and the expression reduces to:

$$f = \left(\frac{1.875^2}{2\pi}\sqrt{\frac{E}{12\rho}}\right)\frac{t}{L^2}$$

For a beam with a proof mass added on the tip, the mass can be modeled as a point load on the tip. The fourth boundary condition then becomes

$$\delta_{xxx}(L,t) = -\frac{m\omega^2}{EI}\delta(L,t),$$

where m is the mass of the beam. The calculation of eigenvalues in this case depends on the ratio of the added mass to the mass of the beam.

3.1.2 Using Stiffness and Effective Mass

If we model the beam deflection as a 1st order spring-mass system, then the resonant frequency can be estimated as

$$f_o = \frac{1}{2\pi}\sqrt{\frac{k_{eff}}{m_{eff}}}$$

The effective mass of the beam itself is approximately 0.236 times the beam's actual mass [18], and if the proof mass is modeled a point load at the tip, the total effective mass is approximately:

$$m_{eff} = 0.236\rho AL + m_{proof}$$

The stiffness of a rectangular beam is $k_{eff} = \frac{3EI}{L^3}$, so for a beam with no proof mass:

$$f = \left(\frac{1}{2\pi}\sqrt{\frac{E}{0.236\cdot 4\rho}}\right)\frac{t}{L^2}$$

Assuming the added mass on the tip is much larger than the mass of the beam itself leads to this expression for the resonant frequency (assuming the stiffness is unaffected):

$$f = \left(\frac{1}{2\pi}\sqrt{\frac{3E}{m_{proof}}}\right)\sqrt{\frac{wt^3}{L^3}}$$

To model the effects of the distributed mass loading, rather than tip loading, of the proof mass, $L_{eff} = L_{beam} - 0.5L_{proof}$ can be substituted for the length.

Both approaches for calculating the resonant frequency arrive at similar results when the proof mass is not taken into consideration, differing by only about 1%. When the proof mass is also considered, the stiffness approach is mathematically simpler, and will be used to estimate the structure size needed to take advantage of ambient vibration sources.

3.2 Modeling of Piezoelectric Generators

3.2.1 Static Deflections

For the modeling of static deflections of beams, a simple equation was derived from the piezoelectric constitutive relationship. DeVoe and Pisano [19] developed a model for multilayer actuators by equating strain at the boundaries of each layer. For this specific beam, a simpler model can be developed exploiting the symmetry of the fabricated structure.

The beams tested have a "sandwich" structure, consisting of alternating layers of aluminum nitride and platinum, as shown in Figure 3.1.

Figure 3.1

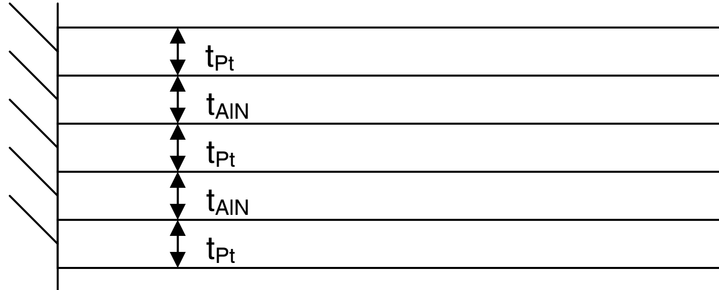

To derive a relationship between deflection of the beam and applied voltage, we start by computing stress based on a known tip deflection. If the tip is deflected downward by some amount δ_t then the deflection along the length of the beam – assuming constant curvature – becomes

$$\delta(x) = -\frac{\delta_t}{L^2}x^2$$

where L is the length of the beam, so that the deflection at x=L is δ_t in the downward direction.

Strain is a linear function of distance from the neutral axis, and is written as

$$S = \frac{M}{EI}y = -\frac{\partial^2 \delta}{\partial x^2}y = \frac{2\delta_t}{L^2}y$$

Figure 3.2 shows this strain variation with respect to the distance from the neutral axis. Using the piezoelectric equation $S = sT + d_{31}\mathbf{E}$, evaluated at $T = 0$, gives the following relationship between the strain, S, and the applied voltage, V.

$$S = \frac{2\delta_t}{L^2}\cdot\frac{1}{2}\left(t_{Pt} + t_{AlN}\right) = d_{31}E = d_{31}\frac{V}{2t_{AlN}}$$

The average distance from the neutral axis is used in place of y to arrive at a value for average stress. In a bending beam, the neutral axis is the line along the beam where no stress is experienced. Because of the symmetric nature of the structure, the neutral axis will be centered vertically.

Figure 3.2

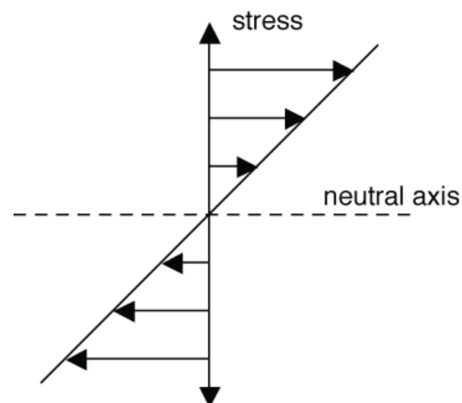

Solving for deflection in terms of voltage gives

$$\delta_t(V) = \frac{d_{31}L^2V}{2t_{AlN}\left(t_{Pt} + t_{AlN}\right)}$$

So deflection as a function of length is then

$$\delta_t(x,V) = \frac{d_{31}x^2V}{2t_{AlN}\left(t_{Pt}+t_{AlN}\right)}$$

Smits and Dalke [20] develop a similar model using energy density to calculate deflection, which reduces to the following for this structure:

$$\delta_t(x,V) = \frac{3d_{31}x^2V}{8t_{AlN}^2}$$

The predictions of the two models and the experimental results are compared in Section 4.2.

3.2.2 Dynamic Deflections

Many different approaches have been used to model the mechanical and electrical behavior of piezoelectric cantilever beam generators when excited by external vibrations [3,5,21,22]. Basic models represent the system as a spring-mass-damper mechanical system, with the electrical output coupled to some physical parameter of the system [3]. More sophisticated models take into account the additional damping and backward coupling effects of the electrical load on the mechanical system [5,21]. Even more accurate models use multiple degrees of freedom to model the effect of mutiple modes of resonance of the system [22].

For this report, the model of Roundy & Wright [5] was chosen for its simplicity and demonstrated success in modeling. A multiple degree of freedom model would provide more accurate results at frequencies far from the first resonant frequency, but near resonance the two should have similar results.

Roundy's model for voltage output across a resistive load, as a function of excitation frequency, is listed below. It is assumed that the two piezoelectric layers are wired in series.

$$\left|V(\omega)\right| = \omega^2\frac{2c_Pd_{31}t_cA_{in}}{\varepsilon k_2}\left\{\left[\frac{\omega_n^2}{RC_b}-\left(\frac{1}{RC_b}+2\zeta\omega_n\right)\omega^2\right]^2+\omega^2\left[\omega_n^2\left(1+k_{31}^2\right)+\frac{2\zeta\omega_n}{RC_b}-\omega^2\right]^2\right\}^{-1/2}$$

The constants in the equation are described in Table 3.1, at the end of this section.

Assuming operation at resonance, Roundy also derives this relationship:

$$\left|V\right| = \frac{2\omega c_Pd_{31}t_cA_{in}}{\varepsilon k_2}\left\{\omega^2\left(\omega^2k_{31}^2+\frac{2\zeta\omega}{RC_b}\right)^2+4\zeta^2\omega^6\right\}^{-1/2}$$

Instantaneous power dissipation is then

$$P = \frac{V_{rms}^2}{R} = \frac{|V|^2}{2R} = \frac{1}{2\omega^2} \frac{RC_b^2\left(\frac{2c_p d_{31} t_c}{k_2 \varepsilon}\right)^2 A_{in}^2}{\left(4\zeta^2 + k_{31}^4\right)\left(RC_b\omega\right)^2 + 4\zeta k_{31}^2\left(RC_b\omega\right) + 4\zeta^2}$$

With an optimal load resistance ($R = 1/\omega C_b$), the power expression becomes

$$P = \frac{1}{2\omega^3} \frac{C_b\left(\frac{2c_p d_{31} t_c}{k_2 \varepsilon}\right)^2 A_{in}^2}{\left(8\zeta^2 + 4\zeta k_{31}^2 + k_{31}^4\right)}$$

Table 3.1:

ω	Driving frequency (in rad/s)
c_P	Young's modulus of piezo layer
t_c	Thickness of piezo layer
A_{in}	Magnitude of input acceleration
ε	Permittivity of piezo layer
k_2	Relates tip deflection to stress: $k_2 = \frac{L^2}{\frac{3}{2}\left(t_{Pt} + t_{AlN}\right)} \frac{2L + \frac{3}{2}L_{mass}}{2L + L_{mass} - L_{electrode}}$
ω_n	Resonant frequency of generator
R	Load resistance
C_b	Capacitance of beam
ζ	Damping ratio
k_{31}	Coupling coefficient: $k_{31}^2 = \frac{d_{31}^2 c_P}{\varepsilon}$

3.3 Effects of Scaling

Roundy & Wright briefly discuss the dependence of power output on device scale, and verify that a larger generator will produce a larger power output [5]. However, they do not investigate the full dependence of power generation on device scale.

To understand how power and scale are related, a relation between device size and resonant frequency must first be derived. From section 3.1.2 we see that for devices with a large tip mass:

$$\omega_o \propto \sqrt{\frac{wt^3}{mL^3}}$$

The other parameters in the power equation have the following dependences on scale:

$$C_b \propto \frac{wL}{t},\ t_c \propto t \text{ and } k_2 \propto \frac{L^2}{t}$$

So then the final power dependence on scale is

$$P \propto \left(\frac{wt^3}{mL^3}\right)^{-3/2} \frac{wL}{t}\left(\frac{t}{\frac{L^2}{t}}\right)^2 = \sqrt{\frac{1}{w}\left(\frac{mL}{t}\right)^3} = w^{-\frac{1}{2}}L^{\frac{3}{2}}t^{-\frac{3}{2}}m^{\frac{3}{2}}$$

This brief scaling study shows that a long, thin beam with a large proof mass will yield the most power. Another interesting result is to consider a base design, with a standardized length, width, thickness, and proof mass size, and investigate what happens when each dimension is scaled linearly. Mathematically, this can be emulated by replacing each linear dimension by a factor of k, and the mass by k^3, since mass is proportional to volume, which is measured in the cube of linear dimensions. It is then derived that power is proportional to the fourth power of the linear dimension of the device, i.e. that

$$P \propto k^4.$$

This also means that power per unit area and volume will both decrease when devices are scaled down, since area and volume are proportional to k^2 and k^3. Kasyap [8] arrives at a similar conclusion and verifies it with finite-element method (FEM) simulations.

4. EXPERIMENTAL RESULTS

4.1 Experimental Setup

For testing purposes, the die containing the cantilevers to be tested was attached to a PCB approximately 4cm by 4cm with carbon tape. Two leads were soldered to the PCB, and the contacts connected to the electrodes on the surface of the beam were wire-bonded to the PCB. On the device itself, the top and bottom electrodes share a single pad on the die, and the second pad is connected to the middle electrode. A hole was drilled in the center of the PCB and threaded for attachment to the mount on the vibration shaker.

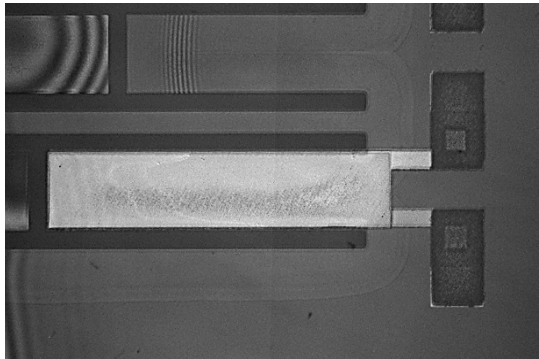

Figure 4.1a: an overhead view of one of the 400μm beams

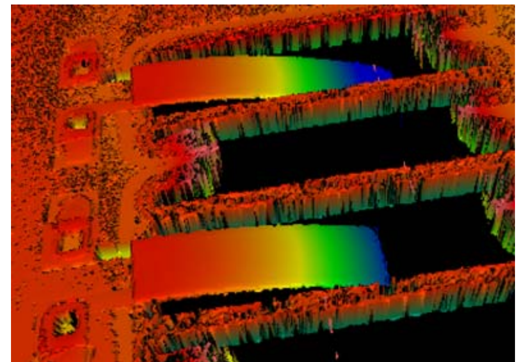

Figure 4.1b: a side view of two beams showing the bending caused by the mass of the beam

Due to the time constraints, the design and fabrication of a generator was not feasible. Instead, a cantilever on an older wafer was chosen for analysis. The cantilever to be tested is approximately 400μm long and 100μm wide, with t_{Pt} = 0.2μm and t_{AlN} = 1μm (see Figure 3.1). There is actually a series of cantilevers, with lengths of 400, 300, 200, and 100 μm. However, the longest cantilever would exhibit the greatest response, so the 400μm was chosen for testing. Since the cantilevers were not designed with energy harvesting in mind, they lacks proof masses. This design is not optimal, but it does serve to illustrate many of the characteristics that would need to be taken into account. The relevant material properties used in estimates can be seen in Table 4.1.

Table 4.1:

E_{AlN} (in plane)	292 GPa [23]
ρ_{AlN}	3200 kg/m^3 [17]
d_{31} (AlN)	-1.98 pC/N [23]
E_{Pt}	168 GPa [17]
ρ_{Pt}	21450 kg/m^3 [17]

4.2 Resonant frequency verification

To verify the estimates for the resonant frequency, the impedance of the device was measured across a range of frequencies using an Agilent impedance analyzer. The impedance measurements were done in a vacuum, as damping due to air would severely reduce the beam's movement at atmospheric pressure and make the resonance peak difficult to discern.

The following measurement was made for the beam measuring 400μm long by 100 μm wide:

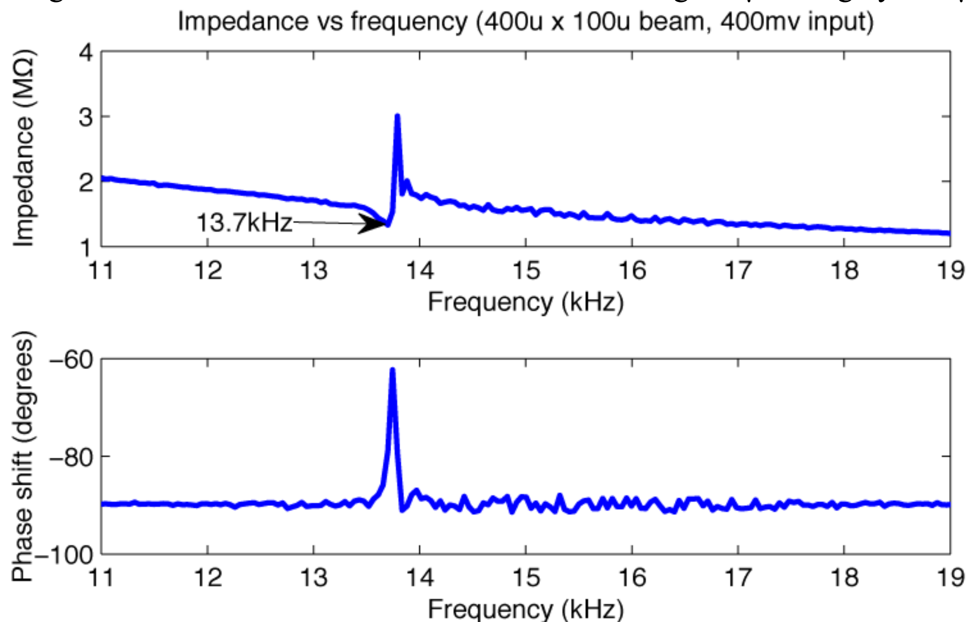

Figure 4.2

Using the approximate relationships derived in section 3.1, the calculated resonant frequencies are 15.6 kHz (beam equation approach) and 15.9 kHz (stiffness approach). This represents errors

of 13% and 15%, respectively. For comparison purposes, another impedance measurement was made of a 300µm by 100µm beam on the same die:

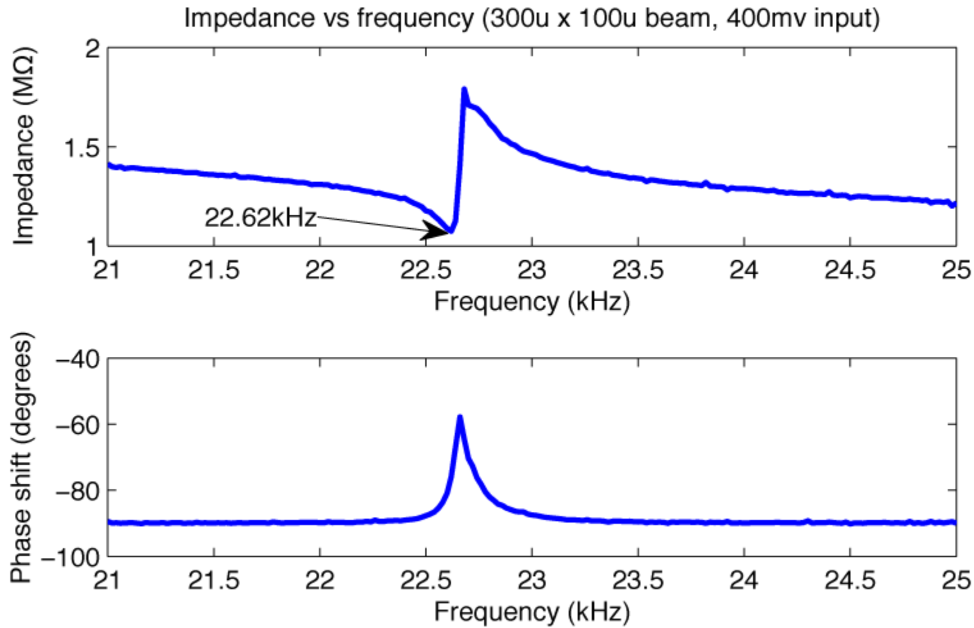

Figure 4.3

In this case, the calculated resonant frequencies are 27.8 kHz (beam equation) and 28.2 kHz (stiffness), and the relative errors are 22% and 25%.

Since the relative error increases significantly when a shorter beam is used, this suggests that the derived models are not as accurate for shorter beams. In fact, one of the assumptions of the Euler-Bernoulli beam equation is that the length is significantly larger than the width and thickness. Keeping all other factors constant, better agreement would be expected with longer beams.

4.2 Static Deflection

To verify the actuation response of the beam, a voltage was applied across the electrodes of the beam and the deflection response measured (see figure 4.4). The measurements were made using a Zygo laser interferometer.

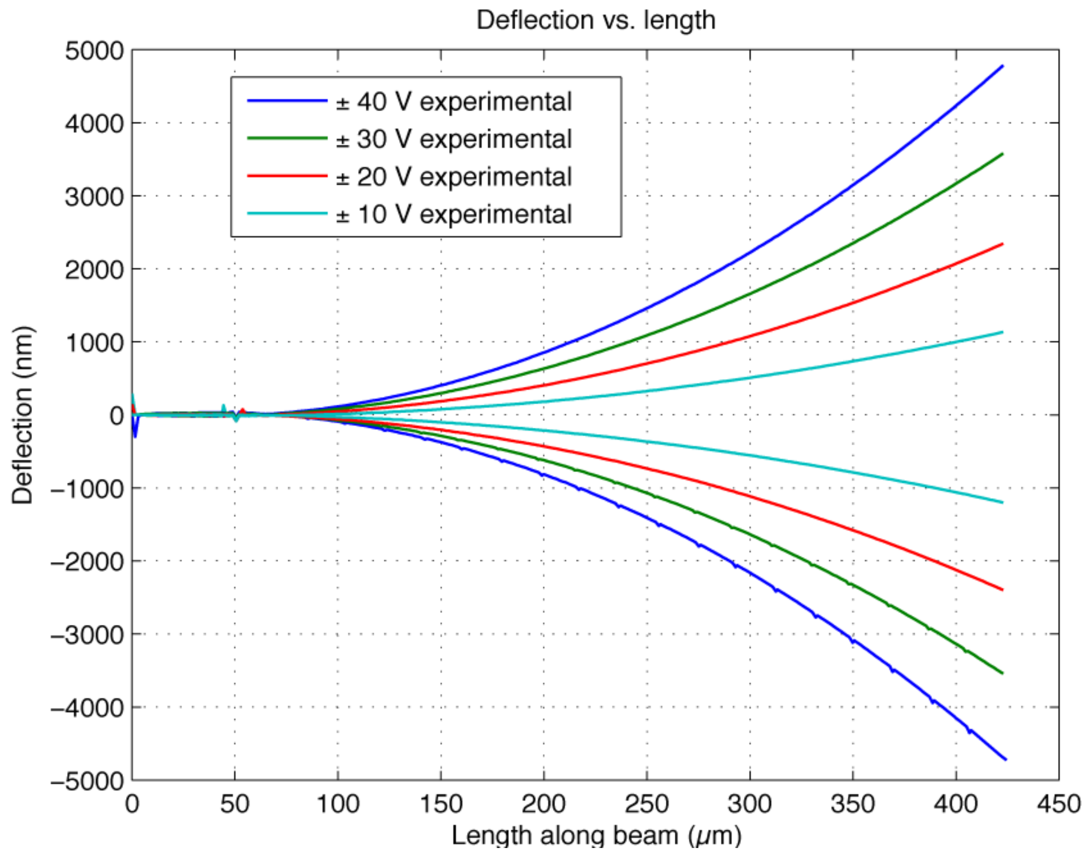

Figure 4.4

Comparing tip deflection between experimental measurements and theoretical predictions shows that the theory overestimates the tip deflection by a small but noticeable amount:

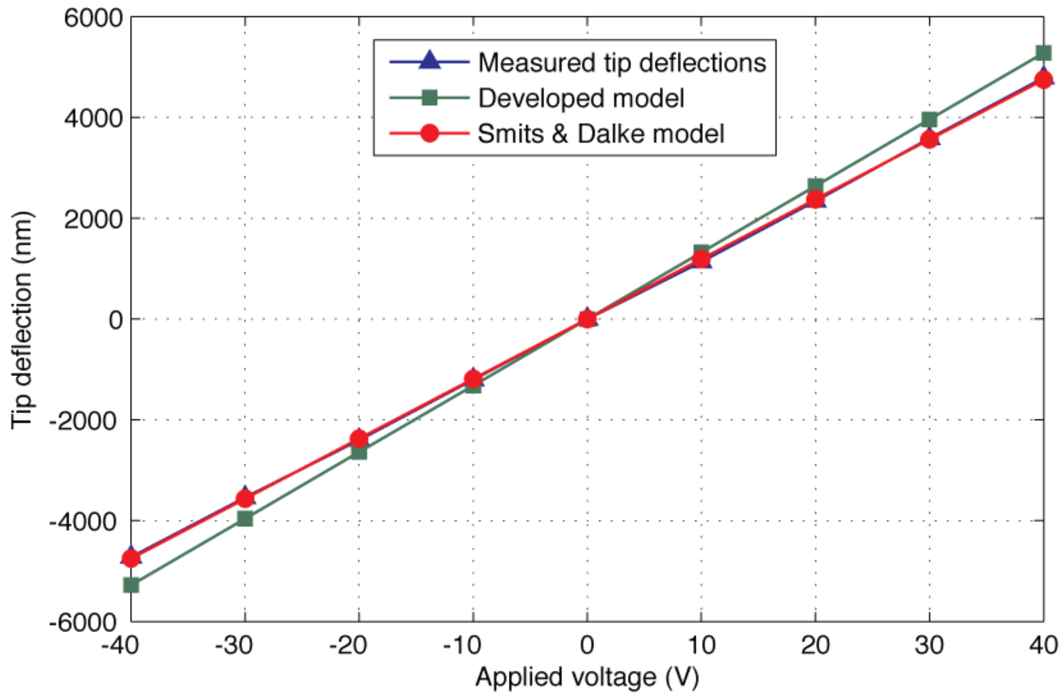

Figure 4.5

The relative error between the developed model and the experimental results is about 10% for each applied voltage. The model derived by Smits & Drake [20] is accurate to within 5% for all data points, and within 1% for most.

4.3 Excitation using Vibration Shaker

To test the beam's response to accelerations, the PCB with the wire-bonded die was fastened securely to the shaker mount. An Agilent function generator was used to drive the shaker, and the output signal from the piezoelectric device was buffered and amplified so it could be measured with an oscilloscope.

However, since the output current of the function generator is limited, sufficient acceleration levels could not be created. Using a Phidgets accelerometer, the applied acceleration was measured and was found to have a magnitude of only about 0.1 g.

In an attempt to resolve this issue, an Apex PA-98 amplifier was also used to drive the shaker. This did result in an improved acceleration output, but the shaker output was then limited by the low current capability of the amplifier (~40mA). To facilitate future testing, an amplifier configuration with a higher output current will be used, as the PA-98 can support up to 200mA of output.

Figure 4.6: Diagram of shaker setup

5. CONCLUSIONS AND RECOMMENDATIONS

It has been shown that the current device structure does not have scaling advantages in power per unit area or volume. It is difficult to produce sufficient displacement at small scales to generate a considerable voltage. At the microscale, resonance frequencies are too low to effectively convert ambient frequencies as found in nature.

As an illustration of the challenge of reaching lower frequencies with MEMS devices, consider a beam of equal width and thickness as the one tested, but a significantly larger length and an added proof mass. Using the frequency estimate in section 3.1.2, a 2000μm by 100μm by 2.6μm

beam would need to have a 0.11mg proof mass to reach even 200 Hz. Using a relatively dense metal such as gold would still require a cubic proof mass of approximately 148μm on each side.

Due to the difficulty in reaching low frequencies with MEMS scale devices, these types of energy harvesters would be limited to applications with very high frequency vibrations. However, for compact systems with very low power requirements, MEMS microgenerators are a very attractive means of powering devices indefinitely.

Recommendations are to build devices of this form, with a proof mass added, while targeting lower resonant frequencies. Alternate geometries may help in lowering the resonant frequency, and gaining more power output. More effective solutions include designing a structure that is either not dependent on resonance, or has a means of tuning its resonant frequency. Examples of such devices have already been demonstrated by other researchers [24,25]. To take advantage of the large deflections and strains that go with a beam oscillating at resonance, the tuning approach is recommended as the most useful for power output. The challenge will be in adapting existing tuning approaches to the MEMS scale, or in devising a new means to tune the beams' resonant frequency.

6. REFERENCES:

1. A. Chandrakasan, R. Amirtharajah, J. Goodman, W. Rabiner, Trends in Low Power Digital Signal Processing, Proceedings of the 1998 IEEE International Symposium on Circuits and Systems (1998) 604 – 607.
2. S. Roundy, P.K. Wright, J. Rabaey, A study of low level vibrations as a power source for wireless sensor nodes, *Computer Communications*, 26 (2003) 1131–1144.
3. C.B. Williams, R.B. Yates, Analysis of a micro-electric generator for Microsystems, *Sensors and Actuators*, 52 (1996) 8-11.
4. D. Shen, J.H. Park, J. Ajitsara, S.Y. Choe, H.C. Wikle III, D.J. Kim, The design, fabrication and evaluation of a MEMS PZT cantilever with an integrated Si proof mass for vibration energy harvesting, *Journal of Micromechanics and Microengineering*, 18 (2008) 055017.
5. S. Roundy, P. K. Wright, A piezoelectric vibration based generator for wireless electronics, *Smart Materials and Structures,* 13 (2004) 1131-1142.
6. M. Marzencki, Y. Ammar, S. Basrour, Integrated power harvesting system including a MEMS generator and a power management circuit, *Sensors and Actuators A*, 145-146 (2008) 363-370.
7. Y.B. Jeon, R. Sood, J.H. Jeong, S.G. Kim, MEMS power generator with transverse mode thin film PZT, Sensors and Actuators A 122 (2005) 16–22.
8. A. Kasyap V.S., Development of MEMS-based Piezoelectric Cantilever Arrays for Energy Harvesting, Ph.D. dissertation, Department of Aerospace Engineering, University of Florida, 2007.
9. IEEE Standard on Piezoelectricity, *Standards Committee of the IEEE Ultrasonics, Ferroelectrics, and Frequency Control Society*, ANSI/IEEE Std 176-1987 (1988).
10. M. Marzencki, S. Basrour, B. Charlot, A. Grasso, M. Colin, L. Valbin, Design and fabrication of piezoelectric micro power generators for autonomous Microsystems, *Proc. Symp. on Design, Test, Integration and Packaging of MEMS/MOEMS DTIP05*, (2005) 299-302.

11. H. A. Sodano, J. Lloyd, D. J. Inman, An experimental comparison between several active composite actuators for power generation, *Smart Materials and Structures*, 15 (2006) 1211-1216.
12. J. Cho, M. Anderson, R. Richards, D. Bahr, C. Richards, Optimization of electromechanical coupling for a thin-film PZT membrane: I. Modeling, *Journal of Micromechanics and Microengineering*, 15 (2005) 1797-1803.
13. S. Roundy, E.S. Leland, J. Baker, E. Carleton, E. Reilly, E. Lai, B. Otis, J.M.Rabaey, P.K. Wright, V. Sundararajan, Improving Power Output for Vibration-Based Energy Scavengers, *IEEE Pervasive Computing*, 4 (2005) 28-36.
14. S.G. Braun, D.J. Ewins, S.S. Rao, Encyclopedia of Vibration, Volumes 1-3. Elsevier. Online version available at: http://knovel.com/web/portal/browse/display?_EXT_KNOVEL_DISPLAY_bookid=1873&VerticalID=0
15. A. Hajati, S.G. Kim, Rectifier-less piezoelectric micro power generator, *Proc. SPIE 6928*, 69281T (2008).
16. G.K. Ottman, H.F. Hofmann, A.C. Bhatt, G.A. Lesieutre, Adaptive Piezoelectric Energy Harvesting Circuit for Wireless Remote Power Supply, *IEEE Transactions on Power Electronics*, 17 (2002) 669-676.
17. P.J. Stephanou, Piezoelectric Aluminum Nitride MEMS Resonators for RF Signal Processing, Ph.D. dissertation, Department of Mechanical Engineering, University of California, Berkeley, 2006.
18. J.W. Yi, W.Y. Shih, and W.H. Shih, Effect of length, width, and mode on the mass detection sensitivity of piezoelectric unimorph cantilevers, *Journal of Applied Physics*, 91 (2002) 1680-1686.
19. D.L. DeVoe, A.P. Pisano, Modeling and Optimal Design of Piezoelectric Cantilever Microactuators, *Journal of Microelectromechanical Systems*, 6 (1997) 266-270.
20. J.G. Smits, S.I. Dalke, The constituent equations of piezoelectric bimorphs, *IEEE Ultrasonics Symposium 1989 Proceedings*, (1989) 781-784.
21. N.E. duToit, B.L. Wardle, S.G. Kim, Design Considerations for MEMS-Scale Piezoelectric Vibration Energy Harvesters, *Integrated Ferroelectrics*, 71 (2005) 121–160.
22. A. Erturk, D.J. Inman, A Distributed Parameter Model for Cantilevered Piezoelectric Energy Harvesters, *Journal of Vibrations and Acoustics*, 041002 (2008).
23. G. Piazza, Piezoelectric Aluminum Nitride Vibrating RF MEMS for Radio Front-End Technology, Ph.D. dissertation, Department of Electrical Engineering and Computer Science, University of California, Berkeley, 2005.
24. V.R. Challa, M.G. Prasad, Y. Shi, F. T. Fisher, A vibration energy harvesting device with bidirectional resonance frequency tenability, *Smart Materials and Structures*, 17 (2008) 1-10.
25. D. Spreeman, B. Folkmer, D. Mintenbeck, Y. Manoli, Novel non-resonant vibration transducer for energy harvesting, *PowerMEMS 2005 Proceedings*, (2005) 144-146.